Targeted zwitterionic near-infrared fluorophores for improved optical imaging

Hak Soo Choi[1], **Summer L. Gibbs**[1], **Jeong Heon Lee**[1], **Soon Hee Kim**[1,2], **Yoshitomo Ashitate**[1], **Fangbing Liu**[1], **Hoon Hyun**[1], **GwangLi Park**[1], **Yang Xie**[1], **Soochan Bae**[3], **Maged Henary**[4], and **John V. Frangioni**[1,5,*]

[1]Division of Hematology/Oncology, Beth Israel Deaconess Medical Center, Boston, MA 02215

[2]WCU Department of BIN Fusion Technology, Chonbuk National University, Jeonju 561-756, South Korea

[3]Cardiovascular Division, Department of Medicine, Beth Israel Deaconess Medical Center, Boston, MA 02215

[4]Department of Chemistry, Georgia State University, Atlanta, GA 30303

[5]Department of Radiology, Beth Israel Deaconess Medical Center, Boston, MA 02215

Abstract

The signal-to-background ratio (SBR) is the key determinant of sensitivity, detectability, and linearity in optical imaging. As signal strength is often constrained by fundamental limits, background reduction becomes an important approach for improving SBR. We recently reported that a zwitterionic near-infrared (NIR) fluorophore, ZW800-1, exhibits low background. Here we show that this fluorophore provides much-improved SBR when targeted to cancer cells or proteins by conjugation with a cyclic RGD peptide, fibrinogen, or antibodies. ZW800-1 outperforms the commercially available NIR fluorophores IRDye800-CW and Cy5.5 *in vitro* for immunocytometry, histopathology and immunoblotting, and *in vivo* for image-guided surgery. In tumor model systems, tumor-to-background ratios of 17.2 are achieved after only 4 h post-injection, compared with 5.1 for IRDye800-CW and 2.7 for Cy5.5. Our results suggest that introducing zwitterionic properties into targeted fluorophores may be a general strategy for improving the SBR in diagnostic and therapeutic applications.

Near-infrared (NIR) fluorophores hold great promise for *in vivo* imaging because of reduced tissue absorbance, scatter and autofluorescence at NIR wavelengths between 700 and 900 nm (reviewed in [1–3]). Two commercially available NIR fluorophores, IRDye 800-CW (CW800) and Cy5.5, have highly hydrophobic cores surrounded by a shell of highly anionic surface charge. This chemical and geometric configuration results in relatively high nonspecific binding *in vitro* and *in vivo*[4–6]. When used *in vivo*, targeted imaging reagents are

often cleared through the liver leading to contamination of the gastrointestinal tract[7] making it difficult to achieve sufficient signal-to-background ratio (SBR), defined as the amount of signal in a region of interest relative to the amount of signal in a neighboring region.

Attempts to improve the SBR through background reduction have mainly focused on creating NIR fluorophores whose signal is modified by the local environment. Two of many examples (reviewed in ref. [8]) include enzyme-activated fluorescent probes[9–12] and pH-sensitive agents that show increased quantum yield after endocytosis and transport to lysosomes[13,14]. In both of these cases, a quencher is released leading to increased signal in response to certain proteases or low pH, respectively. However, none of the approaches to date focus on a fundamental limitation of NIR fluorophores, namely, their nonspecific binding, uptake and retention.

A complementary approach that is applicable to nearly any targeting molecule is to create NIR fluorophores that exhibit low nonspecific binding and, for *in vivo* use, are cleared by renal filtration so as to prevent contamination of the gastrointestinal tract. The hypothesis guiding our work is that targeted zwitterionic molecules, molecules containing evenly spaced and interspersed positive and negative charges, might recapitulate the results seen previously with targeted zwitterionic nanoparticles[15–18]. In that prior work, zwitterionic surface coatings, but not anionic or cationic coatings, resulted in much lower than expected nonspecific uptake.

In a previous study characterizing the properties of NIR fluorophores, we found that the zwitterionic heptamethine indocyanine NIR fluorophore ZW800-1 exhibits low serum binding, ultralow nonspecific tissue background and rapid elimination from the body via renal filtration[19]. Moreover, ZW800-1 has notable optical properties including high extinction coefficient and quantum yield, ensuring maintenance of a high signal.

Here we conjugated the zwitterionic NIR fluorophore ZW800-1 to various targeting ligands and compared these with conjugates made using CW800 and Cy5.5, in a broad spectrum of biomedical optical imaging assays. CW800 and Cy5.5 were chosen for comparison as they have the best reported performance and highest number of citations in the literature to date. Our results suggest that targeted zwitterionic NIR fluorophores outperform conventional NIR fluorophores in a wide variety of *in vitro* and *in vivo* assays.

RESULTS

Physiochemical properties of targeted NIR fluorophores

To create targeted ZW800-1 (emission ≈ 800 nm), CW800 (heptamethine indocyanine with a cyclohexane center that emits at ≈ 800 nm) and Cy5.5 (linear pentamethine that emits at ≈ 700 nm), we covalently conjugated each fluorophore to a cyclic peptide consisting of Arg-Gly-Asp-D-Tyr-Lys (cRGD), which specifically binds integrin $\alpha_v\beta_3$ (Fig. 1a). ZW800-1 was synthesized using a process compatible with good manufacturing practices (Supplementary Fig. 1)[20]. Because of the starting anionic charge, cRGD-CW800 and cRGD-Cy5.5 exhibited net surface charges of −4 and a highly unbalanced (i.e., dipole-like) charge-to-hydrophobicity distribution over their surfaces. In contrast, cRGD-ZW800-1 was very hydrophilic (logD = −9.77), had a net surface charge of 0 and had an extremely well-balanced charge distribution over its surface (Fig. 1a). Molecular modeling (Fig. 1a) suggested that the indole nitrogen may be buried after conjugation and thus would not make a notable contribution to surface charge.

Cell binding assays, histology and immunoblotting

We next confirmed the specificity of targeted NIR fluorescent ligands to the surface of living cancer cells using human melanoma cell lines. All of the targeted fluorophores bound to $\alpha_v\beta_3$-positive M21 cells but not to $\alpha_v\beta_3$-negative M21-L cells (Fig. 1b). However, high background signals from nonspecific binding of cRGD-CW800 and cRGD-Cy5.5 were observed in both cell lines, whereas almost no measurable background signal was detected using cRGD-ZW800-1. To determine whether background reduction would also be seen when using large protein-targeting ligands, we conjugated NIR fluorophores to a secondary antibody (see Supplementary Methods) and tested the NIR fluorescent antibody conjugates on breast cancer cells. Her2 overexpressing MDA-MB-361 breast cancer cells showed specific membrane binding with all three antibody-NIR conjugates (Fig. 1c); however, notably higher background signals were observed in the Her2 negative MDA-MB-231 cells when using secondary antibodies conjugated to CW800 or Cy5.5. In addition, cells stained with only the secondary antibody conjugated to Cy5.5 showed strong nonspecific binding in both breast cancer cell lines.

In histopathology, the gold standard for diagnosing many human diseases, it is difficult to obtain adequate SBR because many antigens are in low abundance or are not highly concentrated. To compare the performance of the three NIR fluorophores for immunostaining, we conjugated each one to an antibody and used it to stain tissue sections (Fig. 2, Supplementary Fig. 3, Supplementary Table 1). Resected human tumor-containing tissues from prostatectomies (Fig. 2a) and mastectomies (Fig. 2b) were fixed, frozen and consecutively cryosectioned for alternating NIR fluorescence and hematoxylin and eosin (H&E) staining. Using primary antibodies specific for the tumor of interest, an unlabeled secondary antibody for amplification and NIR fluorophore-labeled tertiary antibodies, malignant cells could be readily identified. However, antibodies conjugated to CW800 or Cy5.5 demonstrated notable nonspecific background binding even when used at a fluorophore to antibody ratio of 1.2. Increasing the labeling ratio to 2.5 (Supplementary Fig. 3) increased background even further, despite the presence of 0.1% nonionic detergent and 0.1% albumin in all solutions.

Immunoblotting is often used to confirm the presence of target protein in a complex biological sample. By using NIR fluorescent light, background signals from autofluorescence and light scattering of membranes could be greatly reduced. However, challenges and limitations remain with respect to sensitivity and quantitation. The zwitterionic antibody conjugate improved SBR by lowering nonspecific membrane staining and/or eliminating false-positive bands (Supplementary Fig. 4).

Tumor targeting and image-guided surgery

Achieving an adequate tumor-to-background ratio (TBR; the CBR from the tumor divided by the CBR from nearby normal tissue), contrast-to-background ratio (CBR; (signal-system background)/system background), and positive-to-negative tumor ratio (PNR; signal from receptor-positive tumor divided by the signal from a receptor-negative tumor in the same animal) is challenging for most targeted contrast agents. Using a xenograft mouse model containing transplanted human melanoma cells ($T+$; tumor from $\alpha_v\beta_3$-positive M21 cell line vs. $T-$; tumor from $\alpha_v\beta_3$-negative M21-L cell line), we compared the performance of the 3 NIR-conjugated cRGD ligands. After intravenous administration of 100 pmol/g of each NIR-conjugated cRGD into tumor-bearing mice, TBR and SBR of the $\alpha_v\beta_3$-positive xenografts increased over a 4 h observation period. The highest TBR (17.2 ± 1.2), SBR (5.1 ± 0.7) and PNR (4.2 ± 0.9) at 4 h post-injection were achieved using cRGD-ZW800-1 (Fig. 3a). With both cRGD-CW800 and cRGD-Cy5.5, the signal in the $\alpha_v\beta_3$-positive tumors was similar to those from cRGD-ZW800-1, as expected because affinity, extinction coefficient

and quantum yield are similar. However, background in non-tumor tissues and receptor-negative tumors were much higher than those seen with cRGD-ZW800-1 (TBR = 5.1 ± 1.2 and 2.7 ± 1.4; SBR = 2.6 ± 0.2 and 1.4 ± 0.2; PNR = 2.1 ± 1.0 and 1.4 ± 1.1 for cRGD-CW800 and cRGD-Cy5.5, respectively) indicative of lower specificity and selectivity. After 4 h, washout from the tumors occurred. Although background decreased, TBR was 4.8, 2.0 and 1.3 for cRGD-ZW800-1, cRGD-CW800 and cRGD-Cy5.5, respectively by 24 h (Supplementary Fig. 5a). Image-guided surgical resection of major tissues and organs at 4 h revealed extremely low uptake in normal tissues and organs with cRGD-ZW800-1 (Supplementary Fig. 5b). The signal seen in skin with cRGD-ZW800-1 is likely due to the normal expression of integrins in skin[21]. In addition, cRGD-ZW800-1 was eliminated from the body exclusively via renal filtration and was unchanged in urine when analyzed by mass spectrometry, while less than 30% of the other targeted agents were found in urine at 4 h post-injection (data not shown).

We next tested these NIR-conjugated cRGD ligands in liver and lung metastatic tumor models because small metastasestumors are difficult to detect wherever nonspecific background is high. Fluorescence signal intensities at the target tumor were similar using each of the three targeted NIR ligands (Fig. 3b). However, cRGD-ZW800-1 expressed almost no background fluorescence in liver and lung tissues, whereas cRGD-CW800 showed high background in the thoracic wall, abdominal wall and liver, and cRGD-Cy5.5 resulted in elevated background in most tissues including lung, liver, gallbladder, abdominal wall and thoracic wall. The highly saturated signal from stomach is due to autofluorescence at 700 nm.

The identification of occult bleeding (i.e., fibrinogen-positive thrombi) in real-time could permit surgeons to intervene intraoperatively to repair damaged tissue. Thus we tested the ability of NIR-labeled fibrinogen (FBG; FBG-ZW800-1, FBG-CW800, and FBG-Cy5.5; Supplementary Fig. 6) to visualize blot clots in mouse models of bleeding in the stomach (Fig. 3c) and mesenteric vessels (Fig. 3c and Supplementary Fig. 6b)[22]. Because the labeling ratio of fluorophores to fibrinogen is similar ($\approx$ 2.5), similar fluorescence intensities were observed in all of the injected animals. However, the intensity of background signal was notably different. FBG-ZW800-1 accumulated rapidly at the site of thrombus formation and achieved an optimal CBR within 60 min post-injection likely owing to rapid blood clearance of FBG and low nonspecific uptake. In contrast, almost no background reduction was achieved over the same time course by FBG-CW800. Because of autofluorescence at 700 nm, the CBR of FBG-Cy5.5 remained low throughout the entire time course. Overall, the lower background of FBG-ZW800-1, compared to FBG-CW800 and FBG-Cy5.5, contributed to 2- to 5-fold higher CBR at 1 h post-injection in both mucosal and mesenteric sites. Control fluorophores without fibrinogen showed no accumulation at any injury site (data not shown).

DISCUSSION

Surgery is the mainstay of cancer treatment, contributing to the cure of approximately half of all patients diagnosed annually. Although many cancer-targeted contrast agents have been described in the literature and some are available commercially, none perform optimally *in vivo* owing to high nonspecific background. Similarly, *in vitro* diagnostics, such as cell-based assays, histopathology and immunoblotting, are often hampered by high background and, therefore, a relatively low SBR. The only two ways to improve SBR during optical imaging are to raise the signal or lower the background. However, for antigen-targeted NIR fluorophores, there is a fundamental limit to signal strength because of the relatively low number of binding sites and intrinsic properties of the fluorophore such as the extinction coefficient, quantum yield, and excitation fluence rate. Although amplification can be used

to raise low signals for *in vitro* diagnostics, amplification during *in vivo* imaging is often complex and clinically unrealistic.

Our study focused on improving SBR by lowering background. Even though the NIR window of 700–900 nm provides relatively high photon transmission and relatively low autofluorescence, nonspecific binding and/or uptake of conventional NIR fluorophores is the major problem impeding the field. We describe reagents for quantitatively imaging metastatic tumors during surgery, cells on a microscope slide, or bands on an immunoblot with much less background signal than seen when using conventional NIR fluorophores.

Two key findings warrant highlighting. First, the physicochemical structure of a relatively small NIR fluorophore can substantially degrade the performance of both small and large targeting molecules. As shown in Figure 4, when a primary amine is conjugated to a tetra-sulfonated molecule, the single positive charge present at physiological pH is replaced by 3 net negative charges, which can disrupt local protein folding, alter the isoelectric point of the molecule and increase nonspecific binding to cationic surfaces. In a zwitterionic fluorophore, however, the amino acid residue has the same net charge with which it started. Because of the implications of this observation, we tested two different chemical classes of NIR fluorophores in parallel as well as targeting ligands spanning the entire spectrum from small molecules to large proteins. This phenomenon was also seen in cell-based assays, histopathological immunostaining, immunoblotting, *in vivo* tumor imaging and image-guided surgery, suggesting that it is, indeed, a general phenomenon. Although the precise mechanism by which zwitterionic structure lowers background is not known, previous studies suggest a combination of charge shielding[23,24] and minimization of membrane penetration[25,26].

Second, the strategy of using small, polyionic yet net-neutral molecules with geometrically balanced charge for *in vivo* imaging leads to clearance exclusively through the kidney and complete elimination of unbound dose from the body into the urine (Supplementary Fig. 5). This observation could be important not only in optical imaging but also in diagnostic imaging and drug design. Zwitterionic radiometal chelators or zwitterionic fluorinated (or other radiolabeled) ligands could reduce background and improve the SBR in positron emission tomography (PET) and single-photon emission computed tomography (SPECT) imaging. It should be noted that both PET and SPECT technology is already capable of detecting tumors over ten-fold smaller than those imaged clinically today, but cannot achieve this potential because of the high background of conventional radiotracers[27]. Similarly, therapeutic molecules, such as membrane-targeted radiotherapeutics and cytotoxins, could achieve a wider therapeutic window if nonspecific binding to normal cells were avoided through the introduction of zwitterionic chemical structure.

One potential problem with this general strategy for small molecules is that blood half-life might sometimes be too short for adequate target contact when using low-affinity ligands. This can be corrected with an inert bulking domain such as polyethylene glycol (PEG). Species-specific blood elimination rates are also important. In previous studies[19,20], blood half-life and renal clearance of zwitterionic NIR fluorophores were proportional to glomerular filtration rate. Because pigs and humans have similar glomerular filtration rates[28], it is likely that the urine elimination rates seen in pig will be similar to those seen in human models.

ZW800-1 is named "−1" because a final net charge of 0 is achieved after conjugation to a ligand with a "−1" residual charge[19]. NBT: ZW800-1 loses a carboxylate (-1) after formation of the amide bond, leaving the indole nitrogen (+1) as the net charge. If the ligand, after conjugation through its amine, has a −1 charge, then the entire molecule is now

net zero. However, we believe that the delocalized, positively-charged indolium may be buried within the hydrophobic core of the molecule (Fig. 1a) and may not contribute to surface charge in some configurations. In such a case, balanced net surface charge may be the dominant predictor of low background adsorption and uptake. A fundamental question arising from our data is whether geometrical balance of charge over the entire surface of a targeted molecule is necessary. That is, would a molecule having polyionicity and net-neutrality but separation of charge in a more dipole-like geometry exhibit the properties of low nonspecific binding and uptake *in vitro* and *in vivo*? Ongoing studies aim to answer this question and to develop a mathematical model for predicting targeted ligand performance based on physicochemical parameters.

In addition to improving the sensitivity and specificity of fluorescence-based *in vitro* diagnostics, our study is likely to improve image-guided surgery, especially image-guided cancer surgery. In a well-designed optical system, NIR fluorescence has the potential to see collections of tumor cells on the surface of a tissue (i.e., margin positivity) as small as 100 cells or fewer. This level of tumor cell detection is currently only available using postoperative histopathological analysis, which typically takes 3–5 working days to reveal whether margins are positive. An ultralow background and concomitantly higher SBR is the only way to achieve this theoretical level of cancer cell detection.

First-in-human clinical trials of ZW800-1 are in process. From the small- and large-animal data already analyzed, it appears that the dose of targeted zwitterionic NIR fluorophores in humans will fall into an acceptably low range. When dose is scaled by body surface area, which we have found to be the best scaling factor for targeted NIR fluorophores[29,30], 100 pmol/g of ZW800-1 in a 20 g mouse (2 nmol) is equivalent to a human dose of $\approx$ 0.43 mg. This is 58-fold lower than the typical vial size of indocyanine green (25 mg), the only FDA-approved 800 nm fluorophore for use *in vivo*. This calculation suggests that ZW800-1–targeted small molecules will have reasonable human dosing. Because ZW800-1 was engineered to have a single carboxylic acid that facilitates stable amide bond formation to amine-containing targeting ligands, one-step 'modular chemistry for producing cancer-specific, small molecule diagnostic agents[31], as well as one-step conjugation to antibodies and other targeting biomolecules, is possible.

ONLINE METHODS

Preparation of NIR Fluorophore Conjugates

Cyclic pentapeptide cyclo(Arg-Gly-Asp-D-Tyr-Lys; cRGDyK; MW 619.6) was synthesized as previously reported[16,32], and conjugated to NIR fluorophores ZW800-1 (available through the nonprofit FLARE Foundation; www.theflarefoundation.org), CW800 (IRDye800 CW, Li-COR, Lincoln, NE), or Cy5.5 (GE Healthcare, Piscataway, NJ) using *N*-hydroxysuccinimide ester (NHS) chemistry in DMSO. NIR fluorophores were also conjugated to secondary or tertiary IgG (Jackson ImmunoResearch Laboratories, West Grove, PA) and fibrinogen (FBG; MP Biomedicals, Irvine, CA) in PBS, pH 7.8, followed by purification by gel filtration chromatography. *In silico* calculations of the partition coefficient (logD) and surface molecular charge and hydrophobicity were calculated using MarvinSketch 5.2.1 by taking major microspecies at pH 7.4 (ChemAxon, Budapest, Hungary). See Supplementary Methods and Table S1 for detailed chemical conjugation and analyses.

Live Cell Binding Assay

Cells were purchased from ATCC (Manassas, VA, USA) and grown in DMEM or RPMI 1640 (Mediatech, Hermdon, VA) supplemented with 10% FBS and gentamicin (50 mg/mL)

in a humidified incubator at 37°C under 5% CO_2 in air. Cells were seeded onto sterilized 18 mm diameter glass coverslips in 12-well plates (3×10^5 cells per well), and incubated at 37°C for 60 min in the presence of 2 to 20 μM targeted NIR fluorophores. After washing, the slides were observed on a 4-channel NIR fluorescence microscope (see Supplementary Methods).

NIR Immunocytochemistry and Immunohistochemistry

The human breast cancer cell lines MDA-MB-361 and MDA-MB-231 were fixed with 2% paraformaldehyde and incubated in 0.1% Triton X-100 in PBS (PBSt) for 10 min. Cells were blocked in 5% goat serum for 10 min and incubated with 10 μg/mL of rabbit anti-human polyclonal antibody c-erbB-2 oncoprotein (Dako) in PBSt for 2 h. The slides were incubated with 20 nM NIR fluorophore-conjugated goat anti-rabbit secondary antibody (labeling ratio ≈ 1.2) in PBSt for 1 h. After a second fixation step with 2% paraformaldehyde in PBS, membrane NIR fluorescence was analyzed using a multichannel Nikon TE300 fluorescence microscope (see Supplementary Methods). For immunohistochemistry, tissues from prostate and breast biopsies were deparaffinized using a Leica autostainer, followed by antigen retrieval. All incubation and washes were in 0.1% Tween-20 and 0.1% porcine serum albumin in PBS, pH 7.4 (PBSta). The primary AMACR antibody (Dako) and c-erbB-2 oncoprotein (Her2) antibody (Dako) were used for the prostate and breast biopsies, respectively. An unlabeled goat anti-rabbit secondary antibody was incubated for 1 h at room temperature, followed by incubation with the conjugated tertiary antibodies for 1 h at a 250 nM concentration. Antibody conjugates were fixed in place with 2% paraformaldehyde, and the tissues were mounted on microscopy slides.

Animals and Tumor Models

Animals were housed in an AAALAC-certified facility, and all animal studies were performed under the supervision of Beth Israel Deaconess Medical Center's Institutional Animal Care and Use Committee (IACUC) in accordance with approved institutional protocol #155-2008. For the tumor targeting study, 6-week-old (20–30 g) male hairless athymic *nu/nu* mice were purchased from Taconic Farms (Germantown, NY). M21 cells (2×10^6) and M21-L cells (5×10^6) resuspended in 100 μL of Matrigel (BD Bioscience, Bedford, MA) were injected subcutaneously in the left and right flank, respectively. For xenograft tumor models metastatic to liver, Lewis lung carcinoma (LLC; ATCC) cells (1×10^6) without Matrigel were administered into athymic *nu/nu* mice through a slow (1–2 min) intrahepatic injection. For xenograft tumor models metastatic to lung, LLC cells (2×10^6) were administered intratracheally as previously reported[14]. For tumor imaging, 2–10 nmol of NIR-conjugated cRGD in saline was administered intravenously into tumor-bearing mice 4 h prior to imaging. For intraoperative thrombus detection, Sprague-Dawley (SD) male rats weighing 250 to 300 g were purchased from Charles River Laboratories (Wilmington, MA). Prior to surgery, animals were anesthetized with 100 mg/kg ketamine and 10 mg/kg xylazine intraperitoneally (Webster Veterinary, Fort Devens, MA). 1.2 mg FBG conjugates (10 nmol of NIR fluorophore) was injected intravenously in SD rats 30 min after mucosal resection or mesenteric vessel injury, when no active bleeding was present. For controls, the same dose of unconjugated fluorophores with a carboxylic acid form was injected.

Intraoperative Imaging and Statistical Analyses

Animals were imaged using FLARE™ imaging system as described in detail previously[2,33]. At each time point, the fluorescence (FL) and background (BG) intensity of a region of interest (ROI) over each organ/tissue was quantified using custom FLARE™ software. The contrast-to-background ratio (CBR) was calculated as CBR = (FL–BG)/BG, where BG is the

system background (the sum of camera noise and filter light leakage), using ImageJ version 1.45q. All NIR fluorescence images for a particular fluorophore were normalized identically for all conditions of an experiment. That is, for each NIR fluorophore, the image with the strongest signal was optimized for brightness, contrast, and gamma (BCG) then these settings were applied to all other images acquired using that particular fluorophore. For tumor-bearing animals, the tumor-to-background ratio (TBR) was measured using an ROI over the tumor for FL and an ROI over the skin for BG. The positive-to-negative tumor ratio (PNR) was measured using an ROI over the receptor-positive tumor for FL, and the same size and shape ROI over the receptor-negative tumor for BG. At least 5 animals were analyzed at each time point. Statistical analysis was carried out using a one-way ANOVA followed by Tukey's multiple comparisons test. Results were presented as mean ± S.D. and curve fitting was performed using Prism version 4.0a software (GraphPad, San Diego, CA).

Supplementary Material

Refer to Web version on PubMed Central for supplementary material.

Acknowledgments

ABBREVIATIONS

AMACR	α-methylacyl-CoA racemase
BG	Background
CBR	Contrast-to-background ratio
cRGD	cyclo(Arg-Gly-Asp-D-Tyr-Lys)
FBG	Fibrinogen
FL	Fluorescence
FLARE™	Fluorescence-Assisted Resection and Exploration
HD	Hydrodynamic diameter
NHS	*N*-Hydroxysuccinimide ester
NIR	Near-infrared
PNR	Positive-to-negative tumor ratio
ROI	Region of interest
SBR	Signal-to-background ratio
TBR	Tumor-to-background ratio
ZW	Zwitterionic

REFERENCES AND NOTES

1. Frangioni JV. In vivo near-infrared fluorescence imaging. Curr Opin Chem Biol. 2003; 7:626–634. [PubMed: 14580568]

2. Gioux S, Choi HS, Frangioni JV. Image-guided surgery using invisible near-infrared light: fundamentals of clinical translation. Mol Imaging. 2010; 9:237–255. [PubMed: 20868625]

3. Te Velde EA, Veerman T, Subramaniam V, Ruers T. The use of fluorescent dyes and probes in surgical oncology. Eur J Surg Oncol. 2010; 36:6–15. [PubMed: 19926438]

4. Ballou B, et al. Tumor labeling in vivo using cyanine-conjugated monoclonal antibodies. Cancer immunology, immunotherapy : CII. 1995; 41:257–263.

5. Ballou B, et al. Cyanine fluorochrome-labeled antibodies in vivo: assessment of tumor imaging using Cy3, Cy5, Cy5.5, and Cy7. Cancer detection and prevention. 1998; 22:251–257. [PubMed: 9618048]

6. Ye Y, Chen X. Integrin targeting for tumor optical imaging. Theranostics. 2011; 1:102–126. [PubMed: 21546996]

7. Tanaka E, et al. Real-time intraoperative assessment of the extrahepatic bile ducts in rats and pigs using invisible near-infrared fluorescent light. Surgery. 2008; 144:39–48. [PubMed: 18571583]

8. Kobayashi H, Ogawa M, Alford R, Choyke PL, Urano Y. New Strategies for Fluorescent Probe Design in Medical Diagnostic Imaging. Chem Rev. 2009

9. Tung CH, Bredow S, Mahmood U, Weissleder R. Preparation of a cathepsin D sensitive near-infrared fluorescence probe for imaging. Bioconjug Chem. 1999; 10:892–896. [PubMed: 10502358]

10. Achilefu S, et al. Novel bioactive and stable neurotensin peptide analogues capable of delivering radiopharmaceuticals and molecular beacons to tumors. J Med Chem. 2003; 46:3403–3411. [PubMed: 12852770]

11. Lee S, et al. A near-infrared-fluorescence-quenched gold-nanoparticle imaging probe for in vivo drug screening and protease activity determination. Angew Chem Int Ed Engl. 2008; 47:2804–2807. [PubMed: 18306196]

12. Lee S, Park K, Kim K, Choi K, Kwon IC. Activatable imaging probes with amplified fluorescent signals. Chem Commun (Camb). 2008:4250–4260. [PubMed: 18802536]

13. Kobayashi T, et al. Highly activatable and rapidly releasable caged fluorescein derivatives. J Am Chem Soc. 2007; 129:6696–6697. [PubMed: 17474746]

14. Urano Y, et al. Selective molecular imaging of viable cancer cells with pH-activatable fluorescence probes. Nat Med. 2009; 15:104–109. [PubMed: 19029979]

15. Choi HS, et al. Renal clearance of quantum dots. Nat Biotechnol. 2007; 25:1165–1170. [PubMed: 17891134]

16. Choi HS, et al. Design considerations for tumour-targeted nanoparticles. Nat Nanotechnol. 2010; 5:42–47. [PubMed: 19893516]

17. Choi HS, et al. Rapid translocation of nanoparticles from the lung airspaces to the body. Nat Biotechnol. 2010; 28:1300–1303. [PubMed: 21057497]

18. Choi HS, Frangioni JV. Nanoparticles for Biomedical Imaging: Fundamentals of Clinical Translation. Mol Imaging. 2010; 9:291–310. [PubMed: 21084027]

19. Choi HS, et al. Synthesis and in vivo fate of zwitterionic near-infrared fluorophores. Angew Chem Int Ed Engl. 2011; 50:6258–6263. [PubMed: 21656624]

20. Hyun H, et al. cGMP-Compatible preparative scale synthesis of near-infrared fluorophores. Contrast Media Mol Imaging. 2012; 7:516–524. [PubMed: 22991318]

21. Adams JC, Watt FM. Expression of beta 1, beta 3, beta 4, and beta 5 integrins by human epidermal keratinocytes and non-differentiating keratinocytes. J Cell Biol. 1991; 115:829–841. [PubMed: 1918165]

22. Ohnishi S, Garfein ES, Karp SJ, Frangioni JV. Radiolabeled and near-infrared fluorescent fibrinogen derivatives create a system for the identification and repair of obscure gastrointestinal bleeding. Surgery. 2006; 140:785–792. [PubMed: 17084722]

23. Colton IJ, Carbeck JD, Rao J, Whitesides GM. Affinity capillary electrophoresis: a physical-organic tool for studying interactions in biomolecular recognition. Electrophoresis. 1998; 19:367–382. [PubMed: 9551788]

24. Gitlin I, Gudiksen KL, Whitesides GM. Effects of surface charge on denaturation of bovine carbonic anhydrase. Chembiochem. 2006; 7:1241–1250. [PubMed: 16847847]

25. Bourre L, Giuntini F, Eggleston IM, Wilson M, MacRobert AJ. Protoporphyrin IX enhancement by 5-aminolaevulinic acid peptide derivatives and the effect of RNA silencing on intracellular metabolism. Br J Cancer. 2009; 100:723–731. [PubMed: 19240715]

26. Zwaal RF, Comfurius P, van Deenen LL. Membrane asymmetry and blood coagulation. Nature. 1977; 268:358–360. [PubMed: 887167]

27. Frangioni JV. New technologies for human cancer imaging. Journal of clinical oncology : official journal of the American Society of Clinical Oncology. 2008; 26:4012–4021. [PubMed: 18711192]

28. Rasmussen F. Renal clearance: species differences and similarities. Vet Res Commun. 1983; 7:301–306. [PubMed: 6665989]

29. Reagan-Shaw S, Nihal M, Ahmad N. Dose translation from animal to human studies revisited. FASEB J. 2008; 22:659–661. [PubMed: 17942826]

30. Kelley KW, Curtis SE, Marzan GT, Karara HM, Anderson CR. Body surface area of female swine. J Anim Sci. 1973; 36:927–930. [PubMed: 4703721]

31. Humblet V, Misra P, Frangioni JV. An HPLC/mass spectrometry platform for the development of multimodality contrast agents and targeted therapeutics: prostate-specific membrane antigen small molecule derivatives. Contrast Media Mol Imaging. 2006; 1:196–211. [PubMed: 17193697]

32. Chen X, Conti PS, Moats RA. In vivo near-infrared fluorescence imaging of integrin alphavbeta3 in brain tumor xenografts. Cancer Res. 2004; 64:8009–8014. [PubMed: 15520209]

33. Troyan SL, et al. The FLARE™ intraoperative near-infrared fluorescence imaging system: a first-in-human clinical trial in breast cancer sentinel lymph node mapping. Ann Surg Oncol. 2009; 16:2943–2952. [PubMed: 19582506]
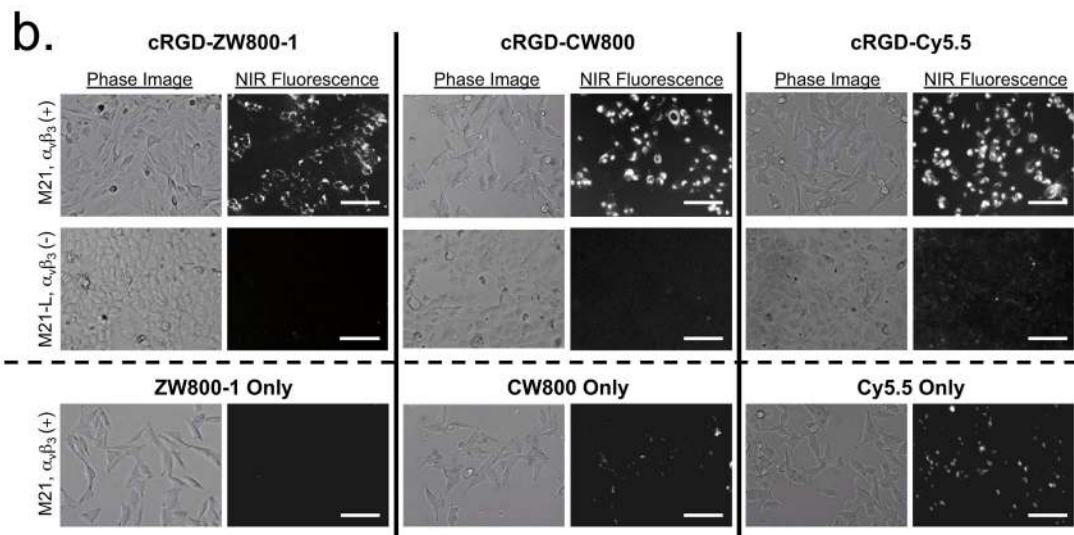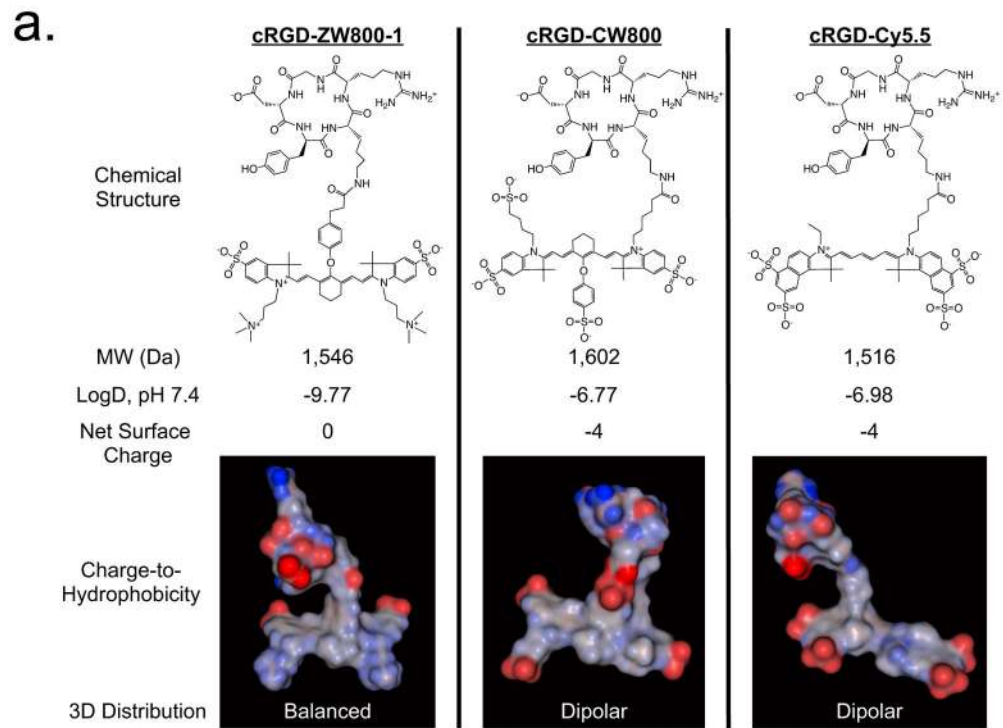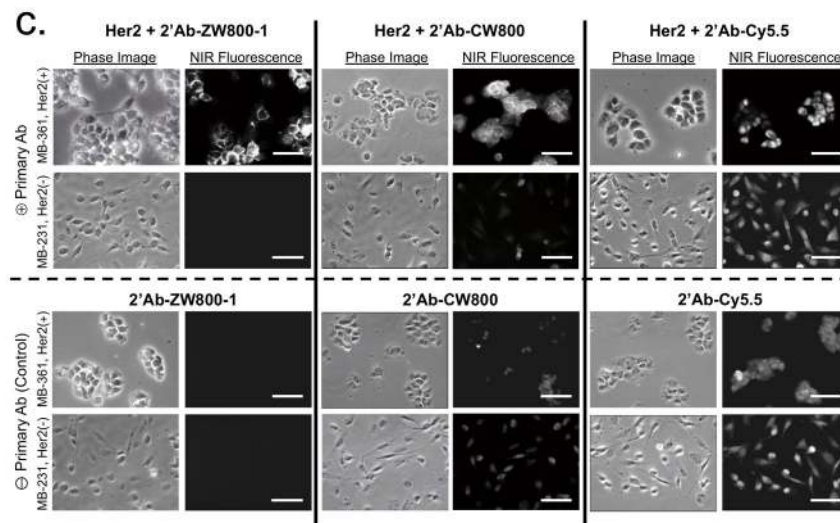
Figure 1. Targeted NIR fluorophores and improved SBR during cell-based assays
(a) Chemical structure, molecular weight (MW), logD, net surface charge and 3D modeling of the geometrical position of charge and hydrophobicity of cRGD-ZW800-1, cRGD-CW800 and cRGD-Cy5.5 at pH 7.4. Red = negative charge; Blue = positive charge; Gray = hydrophobicity.
(b) Live cell binding assay for cRGD-ZW800-1, cRGD-CW800 and cRGD-Cy5.5 (top 2 rows) or NIR fluorophores alone (bottom row) in M21 ($\alpha_v\beta_3$-positive) and M21-L ($\alpha_v\beta_3$-negative) melanoma cell lines after incubation with 2 μM of each molecule for 30 min at 37 C. Scale bars = 100 μm. All NIR fluorescence images have identical exposure times and are normalized to peak signal.
(c) Antibody binding assay for secondary antibodies conjugated with ZW800-1, CW800 and Cy5.5 in MDA-MB-361 (Her2-positive) and MDA-MB-231 (Her2-negative) human breast cancer cell lines in the presence (top 2 rows) or absence (bottom 2 rows) of the anti-Her2 primary antibody. Scale bars = 50 μm. All NIR fluorescence images have identical exposure times and are normalized to peak signal.
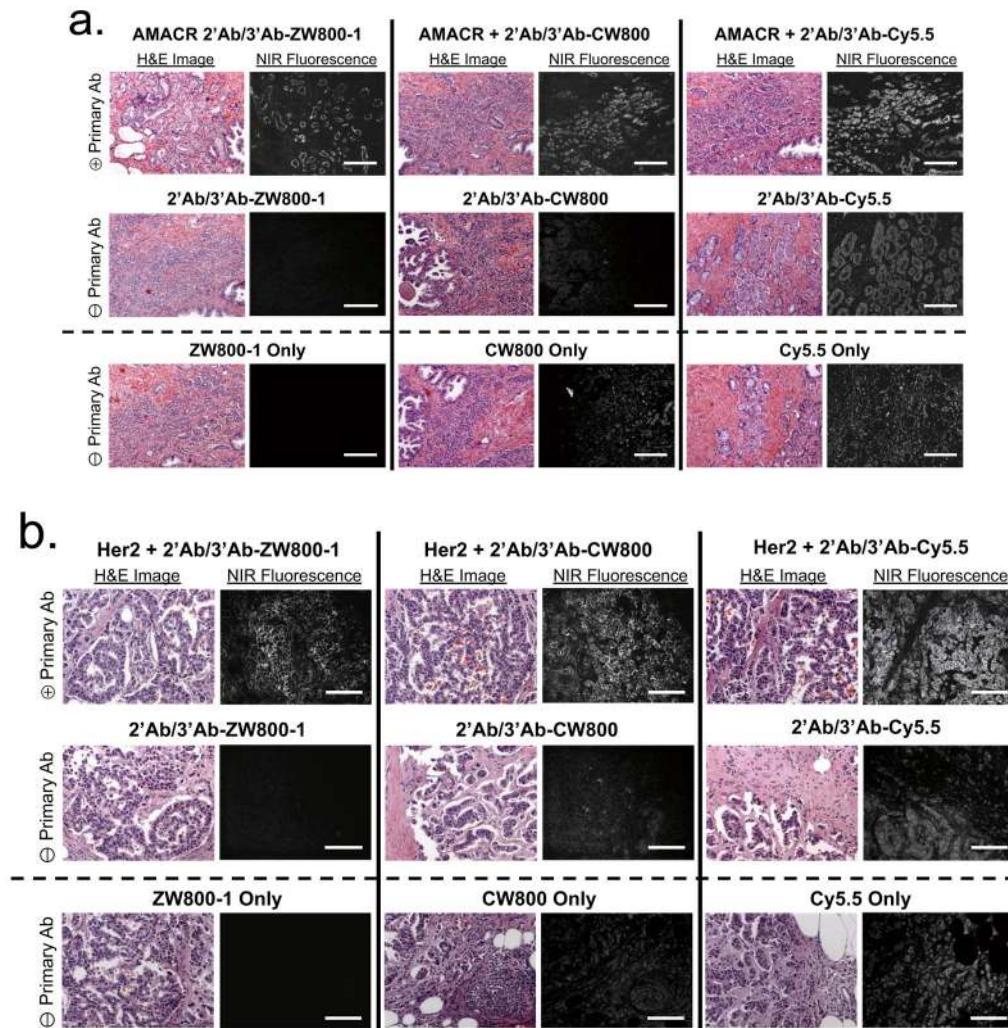
Figure 2. NIR fluorophore-conjugated antibodies and improved SBR during histopathological analysis
(a) H&E (left columns) and NIR fluorescence immunostaining (right columns) of prostate tissue using a rabbit anti-human AMACR primary antibody (top row), goat anti-rabbit secondary and NIR-conjugated mouse anti-goat tertiary antibodies alone (middle row) and NIR fluorophores alone (2 μM each; bottom row). All NIR fluorescence images have identical exposure times and are normalized to peak signal.
(b) H&E (left columns) and NIR fluorescence immunostaining (right columns) of breast tissue using a rabbit anti-human Her2 primary antibody (2 row), goat anti-rabbit secondary and NIR-conjugated mouse anti-goat tertiary antibodies alone (middle row) and NIR fluorophores alone (2 μM each; bottom row). All NIR fluorescence images have identical exposure times and are normalized to peak signal. Scale bars = 200 μm.
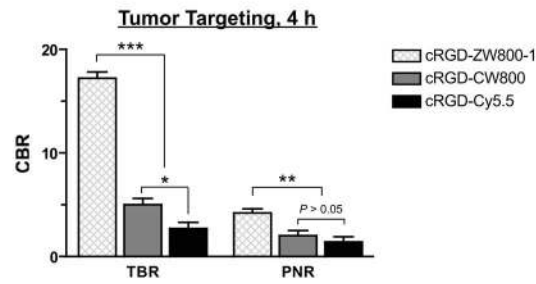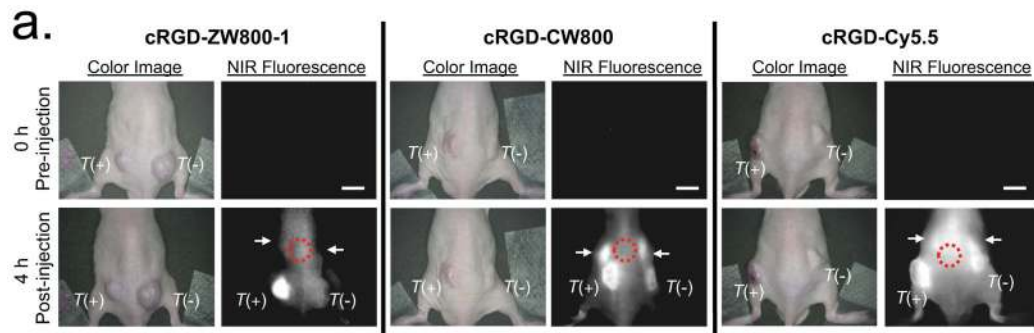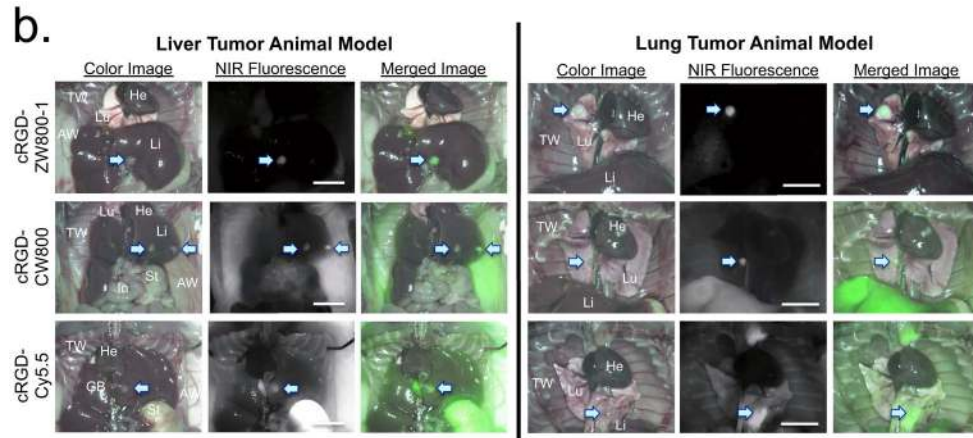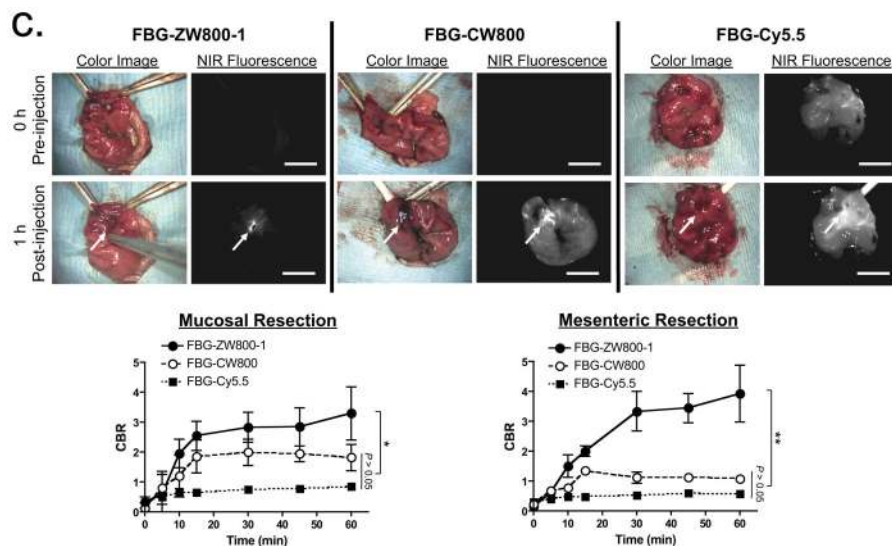
Figure 3. Improved *in vivo* optical imaging using zwitterionic, NIR fluorescent, targeted small molecules and proteins

(a) Real-time intraoperative melanoma detection using targeted small molecules. 3 nmol of cRGD-ZW800-1 (left), 3 nmol of cRGD-CW800 (middle), or 10 nmol of cRGD-Cy5.5 (right) was injected intravenously into melanoma tumor mice. Shown are representative (n = 5) images of color and NIR fluorescence immediately pre-injection (0 h) and at 4 h post-injection. $T(+)$ = integrin $\alpha_v\beta_3$-positive tumor; $T(-)$ = integrin $\alpha_v\beta_3$-negative tumor; arrows = kidneys; red dotted circle = ROI used for TBR background measurement. Quantitation of image signal and background is also shown at 4 h post-injection. All NIR fluorescence images have identical exposure times and are normalized to peak signal.

(b) Real-time intraoperative liver (left) and lung (right) tumor detection using targeted small molecules. 10 nmol of cRGD-ZW800-1 (top), cRGD-CW800 (middle), or cRGD-Cy5.5 (bottom) was injected intravenously into each tumor mouse 4 h prior to imaging. Shown are representative (n = 5) images of color image, NIR fluorescence and a pseudo-colored merge of the two. AW, abdominal wall; GB, gallbladder; He, heart; In, intestine; Li, liver; Lu, lungs; St, stomach; TW, thoracic wall. Arrows = tumors. All NIR fluorescence images have identical exposure times and are normalized to peak signal.

(c) Real-time intraoperative thrombus detection using targeted proteins. 40 pmol/g of FBG-ZW800-1 (left), FBG-CW800 (middle), or FBG-Cy5.5 (right) was injected intravenously into SD rats 1 h after mucosal resection (arrows) in the stomach (shown) or mesenteric vessels (Supplementary Fig. 6). CBR (lower graphs) was calculated from the ratio of the signal at the site of injury site versus nearby normal tissue background. Arrows = injury sites. Statistical analysis was performed using one-way ANOVA followed by Tukey's multiple-comparison test (*$P < 0.05$; **$P < 0.01$). All NIR fluorescence images have identical exposure times and are normalized to peak signal. Scale bars = 1 cm.
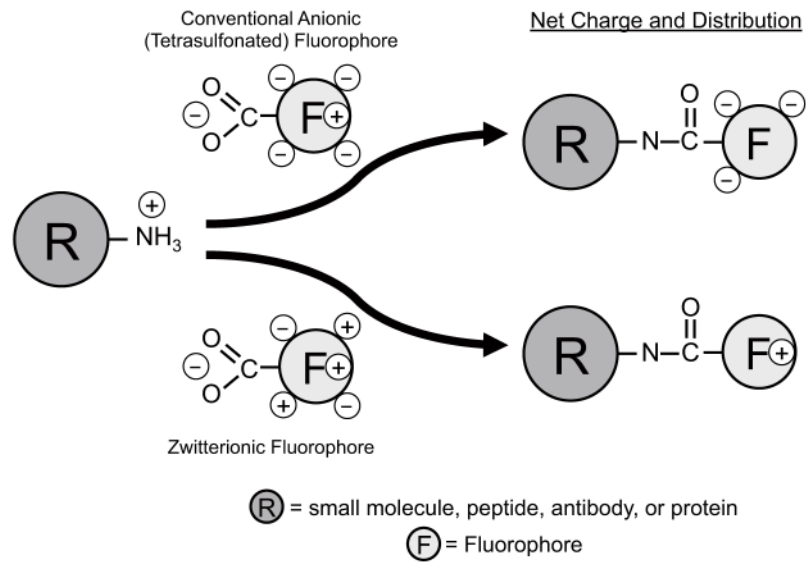
Figure 4.
Modification of a primary amine by commercially available anionic NIR fluorophores (top) and zwitterionic NIR fluorophores (bottom).